

ORIGINAL INNOVATION

Open Access



# Displacement-based seismic performance of RC bridge pier

Javier F. Taipe<sup>1\*</sup>  and Victor I. Fernandez-Davila<sup>2</sup>

\*Correspondence:  
a20173660@pucp.edu.pe

<sup>1</sup> Graduate School, Pontifical Catholic University of Peru, San Miguel, Peru

<sup>2</sup> Faculty of Civil Engineering, Pontifical Catholic University of Peru, San Miguel, Peru

## Abstract

To correctly manage the road infrastructure before and after an earthquake, it is necessary to estimate and even predict the seismic performance of the bridge. The quantification of the bridge's seismic performance response was present in terms of displacement and also based on previous research of reinforced concrete bridge pier models. The displacement did define from a force lateral-displacement response diagram corresponding to the capacity curve, calculated through a non-linear static pushover analysis of the reinforced concrete bridge pier model for each limit state, from intact state to collapse. Thus, six defined displacements correspond to the cracking displacement, the yielding displacement, the spalling displacement, the crushing displacement, the buckling displacement, and the fracturing displacement. The six defined limit states correspond to the cracking limit state, the yielding limit state, the spalling limit state, the crushing limit state, the buckling limit state, and the fracturing limit state. Also, parametric analysis did carry out to evaluate the influence, relative importance, and trend of the input parameters in response to the seismic performance of the reinforced concrete bridge pier model. Eleven input parameters did analyze as the concrete compressive strength, the yield stress of reinforcing steel, the concrete cover thickness, the pier aspect ratio, the configuration of the transverse reinforcement, the spacing of the transverse reinforcing steel, the transversal diameter of the transverse reinforcing steel, the longitudinal reinforcement ratio, the transversal diameter of the longitudinal reinforcing steel, the axial load ratio, and coefficient of subgrade reaction.

**Keywords:** Response of the seismic performance, Capacity curve, Pushover analysis, Reinforced concrete bridge pier model, Limit states, Input parameter

## 1 Introduction

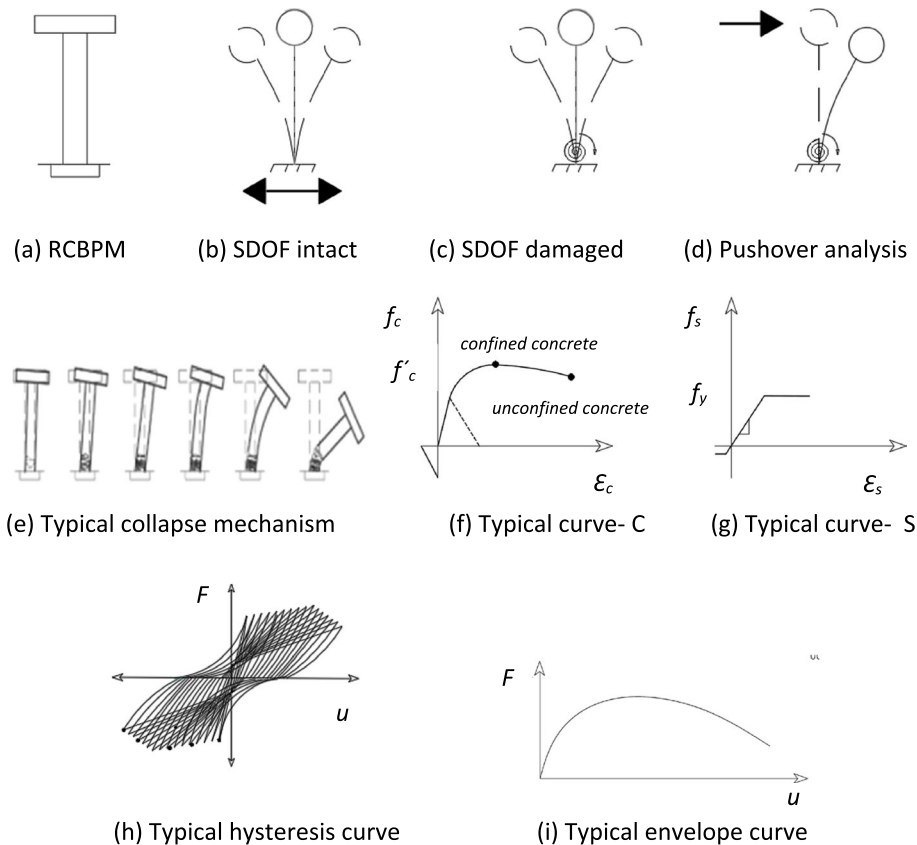
The bridges collapse due to the ground and earthquakes; the bridges collapse due to the ground can be controlled by selecting the appropriate soil and site; however, the bridges collapse due to the earthquake cannot be predicted yet. Vehicular overload and earthquakes are the main factors of bridge damage (Tan et al. 2020; Liu et al. 2022; Li et al. 2020a, b).

The tendency of the collapse of bridges due to earthquakes increases year after year; therefore, it is challenging for engineering to adequately assess the response of the seismic performance of the bridge.

### 1.1 Response of the seismic performance of the bridge

The piers are the most critical components that define the bridges' overall seismic performance; the pier's vulnerability would lead to the bridge's collapse. The seismic performance of the bridge pier corresponds to each damage state expressed in terms of performance levels, generally qualitatively defined as fully operational (damage as cracking only), operational (repairable damage), life safety (damage as resistance degradation), and collapse prevention. Previous works in this regard have used damage indices to quantify the state of damage. Thus, an index value of 0 indicates an undamaged state, and 1 indicates a fully damaged state or failure. Damage states may or may not take into account the effect of cyclic load effect (non-cumulative or cumulative damage indices). The energy-based cumulative damage indices use energy spectra to estimate the influence of cumulative demand on element damage.

The evaluation of the deformation corresponding to the different states of damage requires the evaluation of the force–displacement response envelope (force–displacement model). Thus, the main objective of this paper corresponds to quantify the response of the seismic performance of the reinforced concrete (RC) bridge pier in terms of displacement ( $u$ ). The RC bridge pier model (RCBPM) was proposed for the present work, as schematized in Fig. 1(a). The scaled RC bridge pier specimen consists of the following referential measurements: height of 2.05 m, circular section pier with



**Fig. 1** RCBPM typical capacity curve

a diameter of 0.35m, longitudinal reinforcement ratio of 3%, transversal reinforcement ratio of 2%, concrete compressive strength of 21 MPa, yield stress of reinforcing steel of 412 Mpa, square footing with the size of 0.9m × 0.90 × 0.50m, cap beam with the size of 0.35m × 1.30m.

### 1.1.1 Capacity curve

Generally, due to its simplicity, the intact analytical model of the RCBPM corresponds to an equivalent system of a single degree of freedom (SDOF) (Su et al. 2019, 2015); as schematized in Fig. 1(b). The damaged analytical model of the RCBPM corresponds to the same equivalent system of a simple degree of freedom plus a rotational spring and angle of rotation; the rotational spring exhibits limit state level, rotational spring intact limit state  $\rightarrow \infty$ , damaged limit state close to rotational spring collapse  $\rightarrow 0$ ; as schematized in Fig. 1(c). The nonlinear static pushover analysis of the RCBPM did consider, as schematized in Fig. 1(d). The collapse mechanism of the RCBPM corresponds to each progressive damage state from intact to collapse, as illustrated in Fig. 1(e) (Li et al. 2020a, b). The material laws consider the nonlinearity of the concrete material, as schematized in Fig. 1(f), and the nonlinearity of the steel material, as schematized in Fig. 1(g). The hysteresis curve or the force–displacement–response corresponds to the mathematical representation of the base lateral force versus the lateral displacement of the seismic resistant performance of the RCBPM in a random sequence of loading and unloading as is the case of an earthquake, as schematized in Fig. 1(h). Thus, the capacity curve or the envelope response did obtain from the peak value of the first cycle for each drift ratio in the force–displacement–response; the base shear or lateral force ( $F$ ) did normalize to the weight on the pier, and  $u$  did normalize to height, i.e., drift ratio in percentage as schematized in Fig. 1(i).

### 1.1.2 Reference displacements

The previous similar research conducted by other authors in the literature in which the RC bridge pier's experimental displacement did define as a response parameter did find and ordered lists of some available research in Table 1. Some authors, such as Cassese et al. 2019 only defined two types of displacement ( $u-1$ : intact and  $u-2$ : damaged), and others, such as Pang and Li 2018 defined up to four types of displacement ( $u-1$ : yielding,  $u-2$ : crushing,  $u-3$ : buckling, and  $u-4$ : fracture).

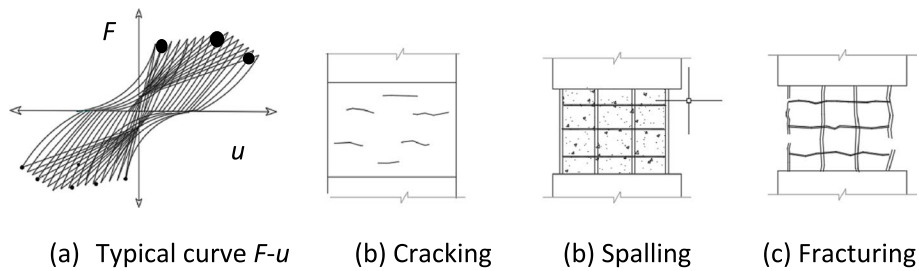
In this regard, drawbacks of the reference displacements were considered, such as the heterogeneity in the type or range of displacements studied, the discontinuity of the research work, and above all, it did not correlate with all damage states (from intact state to collapse). Therefore, in the present manuscript, it did propose that the response of the seismic performance of the RC bridge pier expressed in terms of displacement must correlate with all damage states (from intact state to collapse).

## 1.2 Damage state of RC bridge pier

The performance levels of a bridge correspond to the different states of progressive damage during the seismic performance of the RC bridge pier. During the sequence of damage states, from intact to collapse, there are stages of progressive degradation of the strength and stiffness of the bridge's structural components. In the present

**Table 1** Reference displacements

Author	<i>u-1</i>	<i>u-2</i>	<i>u-3</i>	<i>u-4</i>
Aamir Baig et al. 2022	1.0	1.3	2.0	5.0
Abdallah and El-Salakawy 2022	[2.0, 4.0]	[6.2, 8.2]	10.2	
Cassese et al. 2019	[0.3, 0.8]	[1.5, 2.2]		
Ding et al. 2021	1.0	1.6	4.3	5.5
Afsar Dizaj and Kashani 2020	[0.6, 0.7]	[1.3, 1.9]	[4.8, 5.8]	
Fu et al. 2022	1.0	1.9	4.5	6.7
Jiao et al. 2019	0.6	2.6	4.5	
Kashani et al. 2019	[5.0, 6.0]	[6.2, 9.8]		
Pang and Li 2018	[0.4, 1.0]	[3.6, 5.2]	[9.1, 11.2]	[9.6, 11.8]
Park et al. 2020	0.8	1.2	7.9	8.3
Ren et al. 2022	0.5	2.8	3.7	
Su et al. 2015	[0.8, 1.2]	[1.6, 2.8]	[3.9, 5.1]	
Su et al. 2017a, b	[0.8, 1.2]	[4.3, 5.9]		
Su et al. 2019	[0.8, 1.2]	[4.2, 5.9]		
Su et al. 2020	[0.9, 1.6]	[2.0, 3.2]	[4.1, 4.2]	[4.1, 5.4]
Todorov and Billah 2021	[1.1, 2.9]	[2.3, 4.2]	[2.6, 5.6]	
Todorov and Muntasir Billah 2022a, b	0.2	6.0	9.5	
Tran et al. 2020 ATC-40, FEMA-273	[0.2, 0.5]	[0.5, 1.5]	[1.5, 2.5]	> 2.5



**Fig. 2** Limit states of RC bridge pier

work, the damage states did consider limit states (LS) of the response of the seismic performance of the RCBPM, as schematized in Fig. 2. It is controversial regarding the appearance sequences of concrete cover spalling and longitudinal reinforcement buckling. Some studies assumed that the buckled longitudinal bar would push the concrete cover and then exacerbate spalling of the concrete cover due to its outward deformation trend; hence concrete cover delays or inhibits bar buckling simultaneously. Others indicated that the concrete cover had already spalled off prior to the initiation of bar buckling. Thus, the concrete cover’s effects on bar buckling did reasonably ignored. Traditionally, bridge piers’ limit states did qualitatively define by damage states such as light, moderate, extensive, and complete. However, these now need to be made explicit; future work should focus on studying various levels of earthquakes and structures to establish a good correlation between local and global damage indices.

### 1.2.1 Reference limit state

The previous similar research conducted by other authors searched the literature in which the RC bridge pier’s limit state defined, found, and ordered lists some available research in Table 2. Some authors, such as Srivastava et al. 2022 only defined two types of LS (LS-1: delamination, and LS-2: loss of confinement), and others, such as Kashani et al. 2019 defined up to four types of limit states (LS-1: slight, LS-2: extensive, LS-3: complete, and LS-4: aftershock). In this regard, it did consider that the drawbacks refer to a diversity of qualitative classifications, there is no homogeneity or continuity, and it is not related to the damage in materials (concrete, reinforcement). Therefore, in the present manuscript, it did propose that the limit states of the RCBPM, based on the reference limit states of previous experimental research by other authors, correlated with the damage in the concrete and the reinforcing steel, and that can serve as expected limit states in the future works on RC bridge piers.

### 1.3 Input parameters of the RC bridge pier

In the experimental and analytical investigation, initial parameters or variables did study to characterize the response of the seismic performance of the RC bridge pier to lateral loads. The influence of individual parameters on the force–displacement response of RC bridge piers elements is analyzed. Thus, in the present work, the parameters were considered input parameters (IP).

**Table 2** Reference limit states

Author	LS-1	LS-2	LS-3	LS-4
Cassese et al. 2019	cracking	yielding	peak load	failure
Ding et al. 2021	cracking	spalling	buckling	
Afsar Dizaj and Kashani 2020; Su et al. 2020	yielding	spalling	crushing	
Jiao et al. 2019	crack	spalling	bearing capacity	rebar
Kashani et al. 2019	slight	extensive	complete	aftershock
Pang and Li 2018; Bouazza et al. 2022;	yielding	crushing	buckling	fracture
Park et al. 2020	operational /cracking	immediate occupancy / crushing	life safety /yielding	Collapse Prevention / fracture
Ren et al. 2022	Crack	Yield	Peak	Ultimate
Srivastava et al. 2022	Delamina-tion	Loss of confinement		
Su et al. 2017a, b	cracking	spalling		fracture
Su et al. 2017a, b	Minor	Moderate	Major	failure/ collapse
Todorov and Billah 2021	Repairable	Extensive	Replacement	
Todorov and Muntasir Billah 2022a, b	Cracking	Spalling	Crushing	Buckling
Tran et al. 2020; Aamir Baig et al. 2022	Slight	Moderate	Extensive	Collapse
Zhong et al. 2022	yield of rebar	Elastic-perfectly-plastic	maximum stress of confined concrete	Confined concrete of maximum strain
Zhou and Kunnath 2022	Spalling	Exposed concrete core	Bar buckling (or core shedding)	Multi bar rupture, core crushing

### 1.3.1 Reference input parameters

The previous similar research conducted by other authors searched the literature in which input parameters of the RC bridge pier did define, found, and ordered lists some available research in Table 3. Some authors, such as Anand and Satish Kumar 2018 only defined two types of input parameters (IP<sub>6</sub>: spacing of the transverse reinforcing steel, and IP<sub>11</sub>: coefficient of the subgrade reaction), and others, such as Afsar Dizaj and Kashani 2020 defined up to five types of input parameters (IP<sub>4</sub>: pier aspect ratio, IP<sub>5</sub>: configuration of the transverse reinforcement, IP<sub>6</sub>: spacing of the transverse reinforcing steel, IP<sub>7</sub>: transversal diameter of the transverse reinforcing steel, IP<sub>8</sub>: longitudinal reinforcement ratio, and IP<sub>9</sub>: transversal diameter of the longitudinal reinforcing steel). In this regard, the drawbacks refer to the fact that these generally qualitative conclusions are not yet correlated with the displacements nor with the limit states, besides a limited number of parameters analyzed. Therefore, in the present manuscript, it did propose to analyze the most significant possible number of parameters and analyze their individual and group influence on the response of the seismic performance of the RCBPM and that

**Table 3** Reference input parameters

Author	IP <sub>1</sub>	IP <sub>2</sub>	IP <sub>3</sub>	IP <sub>4</sub>	IP <sub>5</sub>	IP <sub>6</sub>	IP <sub>7</sub>	IP <sub>8</sub>	IP <sub>9</sub>	IP <sub>10</sub>	IP <sub>11</sub>
Aamir Baig et al. 2022		$f_y$		$L/D$				$\rho_l$			
Abdallah and El-Salakawy 2022	$f'_c$			$L/D$						$P$	
Ali et al. 2018					$\emptyset$		$d_t$				
Anand and Satish Kumar 2018						$s$					$k_s$
Barbosa 2015		$f_y$						$\rho_l$			
Cassese et al. 2019				$L/D$							
Ding et al. 2021	$f'_c$	$f_y$	$r$					$\rho_l$	$d_l$	$P$	
Afsar Dizaj and Kashani 2020				$L/D$	$\emptyset$	$s$	$d_t$	$\rho_l$	$d_l$		
Fu et al. 2022		$f_y$	$r$						$d_l$		
Hung et al. 2011											$k_s$
Jiao et al. 2019				$L/D$							
Kashani et al. 2019						$s$					
Kehila and Remki 2015										$P$	
Pang and Li 2018	$f'_c$	$f_y$				$s$		$\rho_l$		$P$	
Park et al. 2020	$f'_c$									$P$	
Ren et al. 2022											
Shelman and Sritharan 2014						$s$					
Su et al. 2015						$s$			$d_l$		
Su et al. 2017a, b		$f_y$									
Su et al. 2019	$f'_c$	$f_y$									
Su et al. 2020		$f_y$						$\rho_l$			
Su et al. 2021		$f_y$									
Todorov and Billah 2021				$L/D$							
Tran et al. 2020				$L/D$							
Xiamuxi et al. 2019					$\emptyset$	$s$			$d_l$		
Zignago and Barbato 2019				$L/D$		$s$					

$f'_c$ : concrete compressive strength;  $f_y$ : yield stress of reinforcing steel;  $r$ : concrete cover thickness;  $L/D$ : pier aspect ratio;  $\emptyset$ : configuration of the transverse reinforcement;  $s$ : spacing of the transverse reinforcing steel;  $d_t$ : transversal diameter of the transverse reinforcing steel;  $\rho_l$ : longitudinal reinforcement ratio;  $d_l$ : transversal diameter of the longitudinal reinforcing steel;  $P$ : axial load ratio;  $k_s$ : coefficient of subgrade reaction or ballast coefficient

they can serve as a categorization of the relevant and irrelevant parameters in future work of RC bridge piers.

### 1.3.2 Regression analysis

A parametric study through the simple linear regression analysis procedure did propose as a statistical technique to model and investigate the relationship between  $u$  (a dependent variable) and input parameters (one independent variable) (Carrasquilla-Batista et al. 2016). Thus, a simple linear regression analysis is performed for only one independent variable, as indicated in Eq. (1).

$$u = \beta_0 + \beta_1 IP \tag{1}$$

where:  $u$  is the dependent variable is also called the explained variable, or response;  $IP$  variable independent variable, also called predictor variable, explanatory variable, regressor;  $\beta_0$  is the intersection of the trend line;  $\beta_1$  is the slope of the line,  $y \in$  represents the random error.

Therefore, in the present manuscript, the impact of each input parameter was determined based on the value of the coefficient of determination ( $R^2$ ). The coefficient of determination is a measure used to explain how much variability of a factor can be caused by its relationship with another related factor. This correlation or goodness of fit is a value between 0 and 1. A value of 1 indicates a perfect fit and, therefore, a very reliable model for future forecasts, while a value of 0 would indicate that the calculation fails to model the data accurately.

Also, a parametric study through the multiple regression analysis procedures did propose a statistical technique to model and investigate the relationship between  $u$  (a dependent variable) and  $IP_k$  (two or more independent variables) (Carrasquilla-Batista et al. 2016). Thus, multiple linear regression analysis did perform for two or more independent variables) Eq. (2).

$$u = \beta_0 + \beta_1 IP_1 + \dots + \beta_k IP_k + \epsilon \tag{2}$$

where:  $IP_1 \dots IP_k$  independent variables, also called predictor variables, explanatory variables, regressors;  $\beta_1 \dots \beta_k$  is the slope of the line.

Therefore, in the present manuscript, the displacement predictor equation was derived based on all the parameters analyzed. This derived multiple linear regression formula can be used in preliminary design when most of the design details are still unknown to determine the feasibility of using the proposed pier to reduce residual displacement (Ou et al. 2022).

Thus, in the present manuscript, the irrelevance of each input parameter was evaluated based on the adjusted coefficient of determination ( $Rr^2$ ). The variation of its value represents this correlation or goodness of fit. It is irrelevant if the  $Rr^2$  value increases by removing the input parameter from the multiple linear regression analysis. It is relevant if the  $Rr^2$  value decreases by removing the input parameter from the multiple linear regression analysis.

## 2 Selection of input parameters and analysis cases

### 2.1 Material

The  $f'_c$  and  $f_y$  did consider input parameters corresponding to the material. The increase in the value of the  $f'_c$  reduced the lateral displacement, as well as improving the capacity to resist the lateral load, the dissipation of the hysteretic energy, and the viscous damping index, according to work developed in this regard by Abdallah and El-Salakawy 2022 and Ren et al. 2022. The nominal  $f'_c$  analyzed 35 MPa, 18 MPa, 21 MPa, 27 MPa, and 35 MPa.

The increase in the value of  $f_y$  increased the lateral displacement, it did not significantly influence the seismic performance, it reduced the amount of steel, it increased the load capacity and hysteretic energy dissipation; according to the works developed in this regard by Barbosa 2015, Su et al. 2021, and Su et al. 2017a, b. The nominal  $f_y$  analyzed 300 MPa, 350MPa, 412MPa, and 549MPa.

### 2.2 Geometry

The  $r$  and  $L/D$  did consider input parameters that correspond to the geometry. The increase in the value of  $r$  did not significantly influence the hysteretic energy dissipation and the strain responses of longitudinal reinforcement. However, it significantly impacted the post-yield stiffness ratio, according to the works developed in this regard by Ding et al. 2021 and Ou et al. 2022. The nominal  $r$  analyzed 0.02 m, 0.03 m, 0.04 m, and 0.05 m.

The increase in the value of the  $L/D$  produced an increase in lateral displacement and a reduction in the basal shear force, as well as the piers with  $L/D$  between 3.8 and 5.4, failed due to flexion, the shorter piers with an  $L/D$  around 2.2 fell per shear; according to the works developed in this regard by (Tran et al. 2020, and Aamir Baig et al. 2022). The nominal  $L/D$  analyzed 4, 6, 8,10.

### 2.3 Transverse reinforcing steel

The  $\emptyset$ , the  $s$ , and the  $d_t$  did consider input parameters corresponding to the transverse reinforcing steel. The  $\emptyset$  or types of stirrups in the pier improved ductility and shear, as well as providing greater confinement, prevented premature buckling of longitudinal reinforcing steel, and increased compressive strength, according to the works developed in this regard by Zignago and Barbato 2019, and Shelman and Sritharan 2014. The nominal  $\emptyset$  analyzed spiral stirrups (ss) and discrete hoops (sh).

The lower value of  $s$  improved ductility and compressive strength. It produced a significant change in the failure mode, according to the works developed by Xiamuxi et al. 2019 and Su et al. 2015. The nominal  $s$  analyzed 0.05 m, 0.10 m, 0.15 m, 0.20 m.

The increase in the  $d_t$  value influenced the deformation, and the adhesion between the concrete and the reinforcing steel, according to work carried out by Ali et al. 2018, and Su et al. 2020. The nominal  $d_t$  analyzed, such as #2, #3, #4, and #5.

### 2.4 Longitudinal reinforcing steel

The  $\rho_l$  and the  $d_l$  did consider input parameters corresponding to the longitudinal reinforcing steel. The increase of the value of  $\rho_l$  increased the lateral displacement; the curvature did reduce, the ductility decreased, and the length of the plastic hinge increased;



according to the works developed in this regard by Bouazza et al. 2022, Fu et al. 2022, and Li et al. 2020a, b. The nominal  $\rho_l$  analyzed 0.7%, 1.5%, 3%, and 4.5%.

The increase in value of  $d_l$  reduced the lateral displacement, as well as adherence slightly decreased; there was an evident influence on the buckling as a function of the relationship between the diameter and the length of the reinforcing steel, according to the works developed in this regard by Wu et al. 2022, and Wang et al. 2022. The nominal  $d_l$  analyzed #2, #3, #4, and #5.

## 2.5 Axial load

The  $P$  is the selected input parameter that corresponds to the weight of the superstructure or the axial load; in this regard, the increase in  $P$  reduced the displacement, as the plastic hinge length increased with axial load, the hysteresis curves for a lower axial load level were slightly tighter than those with a higher axial load level, increased effectiveness of energy dissipation due to higher axial load; according to the works developed in this regard by Jiao et al. 2019, and Kehila and Remki 2015. The nominal  $P$  analyzed 5%, 15%, 20%, and 25%.

## 2.6 Soil-structure interaction

The  $k_s$  is the selected input parameter that corresponds to the soil-structure interaction; in this regard, lower stiffness of the foundation ground resulted in reduced displacement and resistance, as well as the natural frequency of the bridge pier decreased considerably when the pier was damaged, or the foundation stiffness did reduce; according to the works developed in this regard by Hung et al. 2011, Anand and Satish Kumar 2018, Shi et al. 2022, and d'Avila et al. 2022. The nominal  $k_s$  analyzed flexible foundation soil ( $5 \times 105$  N/m<sup>3</sup>), rigid foundation soil ( $5 \times 1010$  N/m<sup>3</sup>),  $1 \times 1011$  N/m<sup>3</sup>, and  $2 \times 1011$  N/m<sup>3</sup>.

As mentioned earlier, the conclusions of the previous research generally correspond to qualitative conclusions. Only a few input parameters did in the study, and they only corresponded to the displacement of a specific limit state. Therefore, another of the proposed objectives of this work corresponds to studying the most significant number of input parameters to analyze their relevance and their trend, corresponding to the displacement of all limit states (from intact to collapse).

The selection of input parameters corresponds to the most studied characteristics of the model of the RC bridge pier on an analytical and experimental basis – most of them were covered. The cases of every parameter correspond to the usual values used in RC issues. The cases analyzed result from combining every parameter and the number of values allocated to each parameter. The eleven input parameters corresponding to the material, geometry, reinforcing steel, axial force, and soil-structure interaction did select, as summarized in Table 4 and Fig. 3.

## 3 Materials and models

### 3.1 Material model

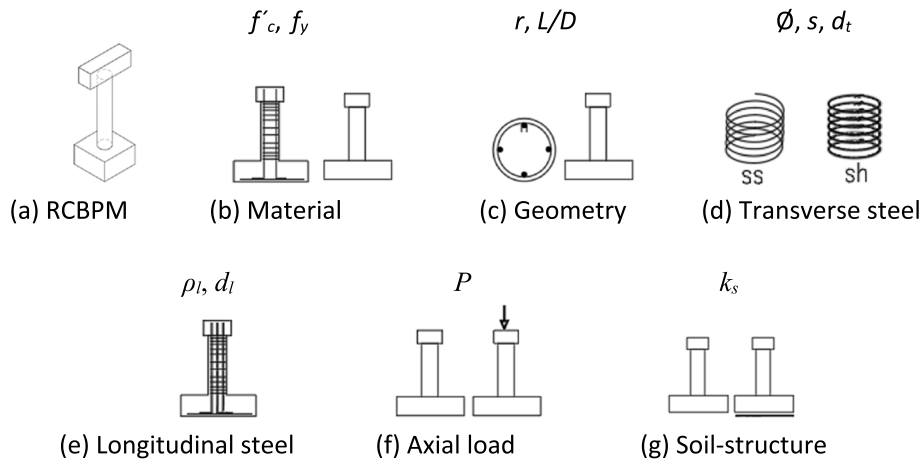
#### 3.1.1 Unconfined concrete

Unconfined concrete (*UC*) refers to concrete (*C*) that did not confine by reinforcing steel (*S*); it did also call covered concrete thickness because it covers the longitudinal

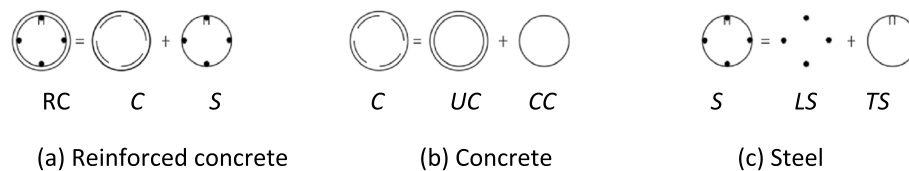
**Table 4** Selected input parameters and analysis cases of the RCBPM

Description	Cases				
Material:	$f'_c$ :	18	<b>21</b>	<b>27</b>	35
	$f_y$ :	300	350	<b>412</b>	<b>549</b>
Geometry	$r$ :	0.02	<b>0.03</b>	<b>0.04</b>	0.05
	$L/D$ :	<b>4</b>	6	<b>8</b>	<b>10</b>
	Transverse reinforcing steel:	$\emptyset$ :	sh	ss	
$s$ :		<b>0.05</b>	<b>0.10</b>	0.15	0.20
Longitudinal reinforcing steel:	$d_t$ :	<b>2</b>	3	<b>4</b>	5
	$\rho_l$ :	<b>0.7</b>	<b>1.5</b>	<b>3</b>	4.5
	$d_l$ :	<b>2</b>	<b>3</b>	4	5
Axial load:	$P$ :	<b>5</b>	<b>15</b>	20	25
Soil-structure interaction:	$k_s$ :	<b><math>5 \times 10^5</math></b>	<b><math>5 \times 10^{10}</math></b>	$1 \times 10^{11}$	$2 \times 10^{11}$

$f'_c$  concrete compressive strength (MPa),  $f_y$  yield stress of reinforcing steel (MPa),  $r$  concrete cover thickness (m),  $L/D$  pier aspect ratio,  $\emptyset$  configuration of the transverse reinforcement,  $s$  spacing of the transverse reinforcing steel (m),  $d_t$  transversal diameter of the transverse reinforcing steel (#),  $\rho_l$  longitudinal reinforcement ratio (%),  $d_l$  transversal diameter of the longitudinal reinforcing steel (#),  $P$  axial load ratio (%),  $k_s$  coefficient of subgrade reaction (N/m<sup>3</sup>)



**Fig. 3** Selected input parameters of the RCBPM



**Fig. 4** Material model

reinforcing steel (*LS*) and transverse reinforcing steel (*TS*) with concrete; it constitutes one of the components of the concrete as specified in Fig. 4(b), and also contributes to the strength of the RCBPM as specified in Eq. (3) and Eq. (4) (Zhong et al. 2022; Zhou and Kunnath 2022).

### 3.1.2 Confined concrete

Confined concrete (*CC*) refers to concrete that is confined by longitudinal reinforcing steel and transverse reinforcing steel, and it did also call concrete core because it did confine by reinforcing steel; it constitutes one of the components of the concrete as specified in Fig. 4(b), and also contributes to the strength of the RCBPM as specified in Eq. (3) and Eq. (4) (Zhong et al. 2022; Zhou and Kunnath 2022).

### 3.1.3 Longitudinal reinforcing steel

Longitudinal reinforcing steel (*LS*) refers to the primary steel along the bridge pier, and it did also measure by amount; it constitutes one of the components of reinforcing steel as specified in Fig. 4(c) and also contributes to the strength of the RCBPM as specified in Eq. (3) and Eq. (4) (Zhong et al. 2022; Zhou and Kunnath 2022).

### 3.1.4 Transverse reinforcing steel

Transverse reinforcing steel (*TS*) refers to the transverse, horizontal, or shear steel that, together with the longitudinal steel, confines the concrete core; it is another component of reinforcing steel as specified in Fig. 4(c) and also contributes to the strength of the RCBPM as specified in Eq. (3) and Eq. (4) (Zhong et al. 2022; Zhou and Kunnath 2022).

$$R = C + S \quad (3)$$

$$R = (UC + CC) + (LS + TS) \quad (4)$$

## 3.2 Limit states

### 3.2.1 The cracking limit state (*LS<sub>1</sub>*)

It corresponds to the first defined limit state, also called damage control, minimal, and slight (Jiao et al. 2019; Park et al. 2020; Todorov and Billah 2021; Hung et al. 2011). The damage status did define according to the material model as the *UC* with cracking initiation, the *CC* undamaged, the *LS* undamaged, and the *TS* undamaged. The resistance is defined as  $R = UC + CC + LS + TS$ , as illustrated in the second column of Table 5.





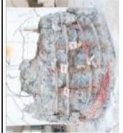

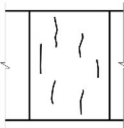
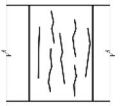

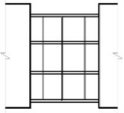
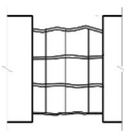
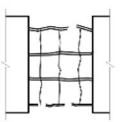
### 3.2.2 The yielding limit state (*LS<sub>2</sub>*)

It corresponds to the second defined limit state, called minor spalling, repairable, and moderate (Todorov and Billah 2021; Zhou and Kunnath 2022; Todorov and Muntasir Billah 2022a). The damage status did define according to the material model: the *UC* with extensive cracking, the *CC* with cracking initiation, the *LS* with yielding initiation, and the *TS* undamaged. The resistance is defined as  $R = CC + LS + TS$ , as illustrated in the third column of Table 5.

### 3.2.3 The spalling limit state (*LS<sub>3</sub>*)

It corresponds to the third defined limit state, life safety, and significant spalling, representing damage with loss of concrete cover (Srivastava et al. 2022). The damage status is defined according to the material model as the *UC* with full spalling, the *CC* with cracking initiation, the *LS* with yielding, and the *TS* with yielding initiation. The resistance is defined as  $R = CC + LS + TS$ , as illustrated in the fourth column of Table 5.

**Table 5** Limit state definition

LS:	LS <sub>1</sub>	LS <sub>2</sub>	LS <sub>3</sub>	LS <sub>4</sub>	LS <sub>5</sub>	LS <sub>6</sub>
	Cracking	Yielding	Spalling	Crushing	Buckling	Fracturing
View:						
Scheme:						
R:	UC+CC+LS+TS	CC+LS+TS	CC+LS+TS	LS+TS	LS+TS	0

### 3.2.4 The crushing limit state ( $LS_4$ )

It corresponds to the fourth defined limit state, life safety, crushing the concrete core (Hung et al. 2011; Todorov and Muntasir Billah 2022b; Srivastava et al. 2022). The damage status is defined according to the material model as the *UC* with full spalling, the *CC* with full cracking, the *LS* with extensive yielding, and the *TS* with yielding. The resistance is defined as  $R = LS + TS$ , as illustrated in the fifth column of Table 5.

### 3.2.5 The buckling limit state ( $LS_5$ )

It corresponds to the fifth defined limit state, also called limited safety, near collapse, extensive, and severe (Kashani et al. 2019; Su et al. 2019; Todorov and Billah 2021). The damage status did define according to the material model: the *UC* with full spalling, the *CC* with full cracking, the *LS* with buckling, and the *TS* with complete yielding. The resistance is defined as  $R = LS + TS$ , as illustrated in the sixth column of Table 5.

### 3.2.6 The fracturing limit state ( $LS_6$ )

It corresponds to the sixth and last defined limit state, also called collapse, fracture, irreparable, and replacement; it represents the state of collapse damage with the fracture of the reinforcement and collapse steel (Kashani et al. 2019; Su et al. 2019; Todorov and Billah 2021). The damage status did define according to the material model: the *UC* with full spalling, the *CC* with full cracking, the *LS* with fracturing, and the *TS* with buckling. The resistance is defined as  $R = 0$ , as illustrated in the seventh column of Table 5.

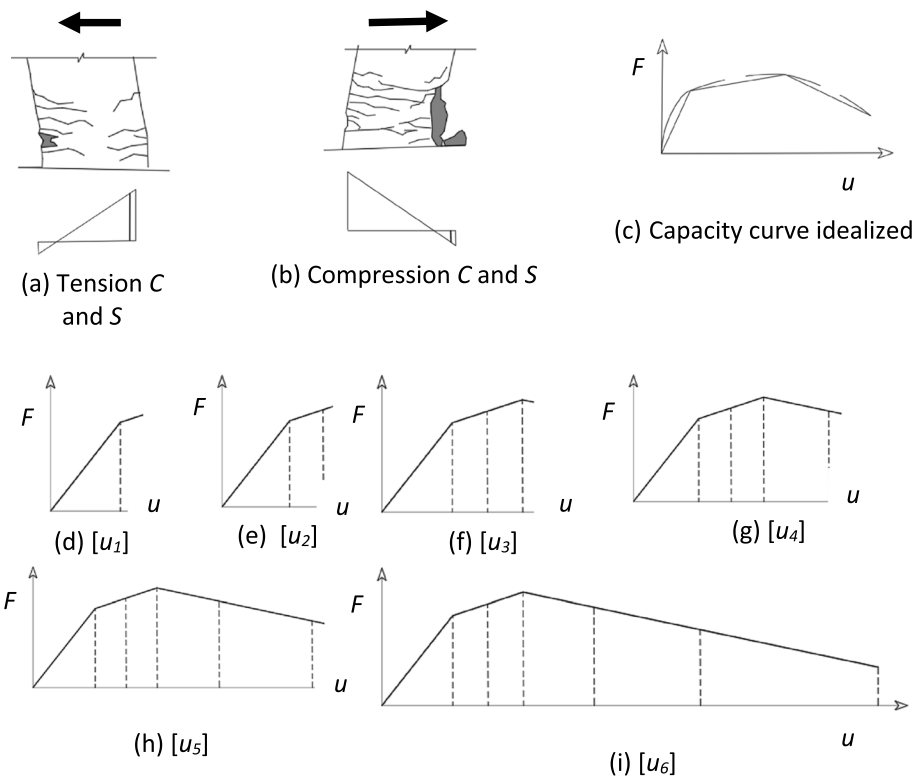
## 3.3 Displacement

### 3.3.1 Cracking displacement ( $[u1]$ )

The first defined displacement interval corresponds to  $LS_1$  (Cassese et al. 2019). The tensile strain does not exceed the maximum strain of concrete and does not exceed the yield strain in reinforcing steel. The compressive strain does not exceed the maximum strain of concrete and does not exceed the yield strain in reinforcing steel. The tensile stress distribution does not exceed the allowable stresses in the concrete and does not exceed the allowable stresses in the reinforcing steel, as schematized in Fig. 5(a) and (b). The displacement interval corresponds to the first line of the trilinear relationship that passes from zero and ends at the idealized yield point (initial stiffness) of the idealized capacity curve (proposed trilinear relationship similar to Federal Emergency Management Agency (FEMA) Standard 356 (2000) (Ou et al. 2022)); as schematized in Fig. 5(c) and (d).

### 3.3.2 Yielding displacement ( $[u2]$ )

The second defined displacement interval corresponds to  $LS_2$  (Kashani et al. 2019; Afsar and Kashani 2020). The tensile strain reaches the maximum strain of concrete and the yield strain in reinforcing steel. The compressive strain does not exceed the maximum strain of concrete and does not exceed the yield strain in reinforcing steel. The tensile stress distribution exceeds the allowable stresses in the concrete and the allowable stresses in the reinforcing steel, as schematized in Fig. 5(a) and (b). The displacement interval corresponds to the first stretch of the second line, beginning from the idealized yield point and ending at the maximum lateral force on the envelope response



**Fig. 5** Displacement definition

(post-yield stiffness) of the idealized capacity curve (proposed trilinear relationship similar to the Federal Emergency Management Agency (FEMA) Standard 356 (2000) (Ou et al. 2022)); as schematized in Fig. 5(c) and (e).

### 3.3.3 Spalling displacement ([u3])

The third defined displacement interval corresponds to  $LS_3$  (Cassese et al. 2019). The tensile strain does exceed the maximum strain of concrete and does exceed the yield strain in reinforcing steel. The compressive strain reaches the maximum strain of concrete and the yield strain in reinforcing steel. As schematized in Fig. 5(a) and (b), the tensile stress distribution reaches maximum stresses in the concrete and yields stresses in the reinforcing steel. The displacement interval corresponds to the second stretch of the second line, beginning from the idealized yield point and ending at the maximum lateral force on the envelope response (post-yield stiffness) of the idealized capacity curve (proposed trilinear relationship similar to the Federal Emergency Management Agency (FEMA) Standard 356 (2000) (Ou et al. 2022)); as schematized in Fig. 5(c) and (f).

### 3.3.4 Crushing displacement ([u4])

The fourth defined displacement interval corresponds to  $LS_4$  (Hung et al. 2011). The tensile strain does exceed the maximum strain of concrete and does exceed the yield strain in reinforcing steel. The compressive strain does exceed the maximum strain of concrete and does exceed the yield strain in reinforcing steel. The tensile stress distribution exceeds the maximum stresses in the concrete and the maximum stresses in the

reinforcing steel, as schematized in Fig. 5(a) and (b). The displacement interval corresponds to the first stretch of the third line, beginning from the maximum lateral force point and ending at the ultimate drift or collapse on the envelope response (post-maximum lateral force stiffness) of the idealized capacity curve (proposed trilinear relationship similar to the Federal Emergency Management Agency (FEMA) Standard 356 (2000) (Ou et al. 2022)); as schematized in Fig. 5(c) and (g).

### 3.3.5 Buckling displacement ( $[u5]$ )

The fifth defined displacement interval corresponds to LS5 (Kashani et al. 2019). The tensile strain does exceed the maximum strain in reinforcing steel. The compressive strain does exceed the maximum strain of strain in reinforcing steel. As schematized in Fig. 5(a) and (b), the tensile stress distribution exceeds the maximum stresses in the reinforcing steel. The displacement interval corresponds to the second stretch of the third line, beginning from the maximum lateral force point and ending at the ultimate drift or collapse on the envelope response (post-maximum lateral force stiffness) of the idealized capacity curve (proposed trilinear relationship similar to the Federal Emergency Management Agency (FEMA) Standard 356 (2000) (Ou et al. 2022)); as schematized in Fig. 5(c) and (h).

### 3.3.6 Fracturing displacement ( $[u6]$ )

The sixth and last defined displacement interval corresponds to LS<sub>6</sub> (Kashani et al. 2019). The tensile strain does exceed the maximum strain in reinforcing steel. The compressive strain does exceed the maximum strain of reinforcing steel. As schematized in Fig. 5(a) and (b), the tensile stress distribution exceeds the maximum stresses in the reinforcing steel. The displacement interval corresponds to the third and last stretch of the third line, beginning from the maximum lateral force point and ending at the ultimate drift or collapse on the envelope response (post-maximum lateral force stiffness) of the idealized capacity curve (proposed trilinear relationship similar to Federal Emergency Management Agency (FEMA) Standard 356 (2000) (Ou et al. 2022)); as schematized in Fig. 5(c) and (i).

## 4 Model results

### 4.1 Model displacement ( $[u_{cal}]$ )

The input parameters, as well as their respective nominal values, are taken into account in the calculation. They are shown in bold and italics in Table 4, with which 4608 model displacement results did achieve. Thus, to evaluate the amplitude of the  $[u_{cal}]$  found, the minimum model displacement ( $u_{min}$ ) and the maximum model displacement ( $u_{max}$ ) were summarized in the second and third rows of Table 6, respectively. The nominal minimum model displacement results from  $u_{min-1}=0.1$ , and the nominal maximum model displacement results from  $u_{max-1}=1.7$  corresponding to LS<sub>1</sub>, the nominal minimum displacement  $u_{min-2}=0.4$  and the nominal maximum displacement  $u_{max-2}=2.3$  corresponding to the LS<sub>2</sub>, up to the nominal minimum displacement  $u_{min-6}=0.4$  and the nominal maximum displacement  $u_{max-6}=3.8$  corresponding to the LS<sub>6</sub>. An increasing trend of their respective amplitude of intervals did observe in the last three limit states. These results did like attributed to the instability of the last damage states.

**Table 6** Displacement results

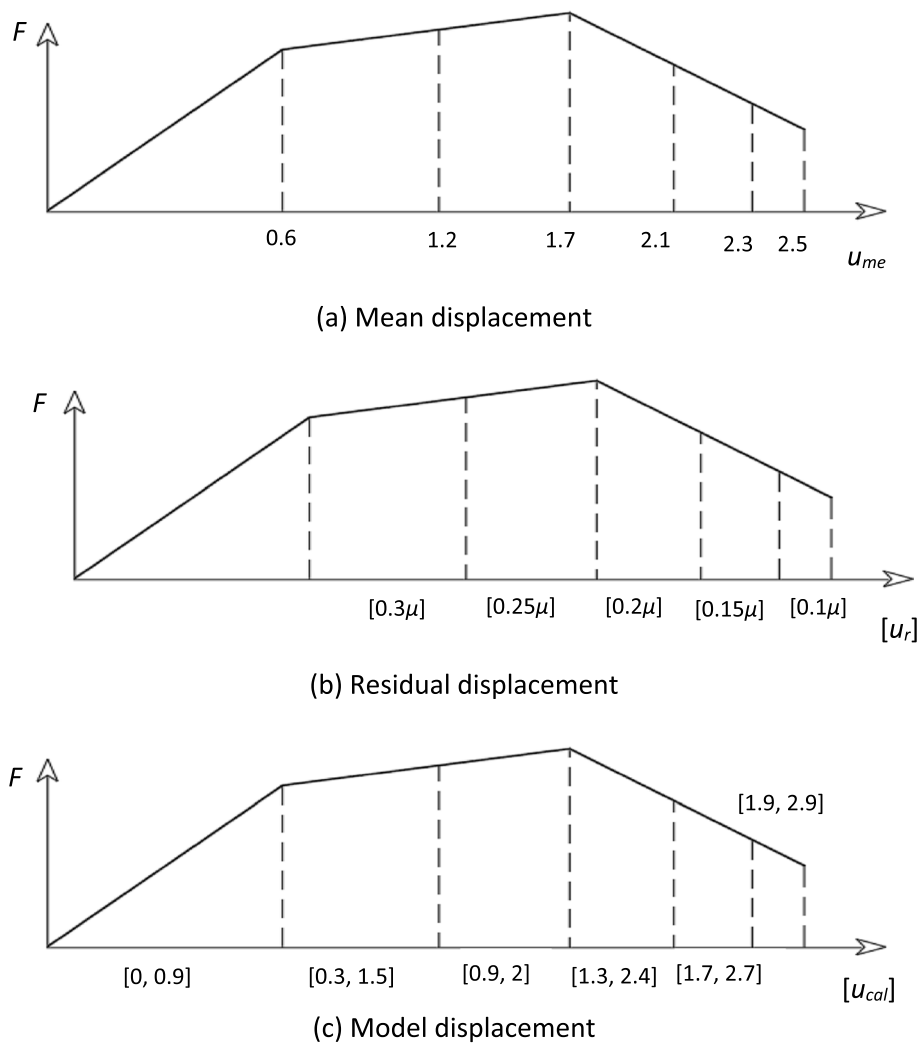
Limit state:	Cracking	Yielding	Spalling	Crushing	Buckling	Fracturing
$u_{min}$ :	0.1	0.4	0.4	0.4	0.4	0.4
$u_{max}$ :	1.7	2.3	2.9	3.3	3.6	3.8
$u_{me}$ :	0.6	1.2	1.7	2.1	2.3	2.5
$[u_r]$ :		$[0.30\mu]$	$[0.25\mu]$	$[0.20\mu]$	$[0.15\mu]$	$[0.10\mu]$
$[u_{cal}]$ :	$[0, 0.9]$	$[0.3, 1.5]$	$[0.9, 2]$	$[1.3, 2.4]$	$[1.7, 2.7]$	$[1.9, 2.9]$
$[u_{ref}]$ :	$[0, 0.4]$	$[1.2, 1.9]$	$[1.9, 2.9]$	$[3.9, 5.4]$	$[5.8, 8.3]$	$[9.3, 10]$
$[u]$ :	$[0, 0.7]$	$[0.8, 1.7]$	$[1.4, 2.5]$	$[2.6, 3.9]$	$[3.8, 5.5]$	$[5.6, 6.5]$

To configure the idealized capacity curve, the mean displacement ( $u_{me}$ ) for each limit state, summarized in the fourth row of Table 6, as follows: the nominal mean displacement  $u_{me-1} = 0.6$  corresponding to the  $LS_1$ , the nominal mean displacement  $u_{me-2} = 1.2$  corresponding to the  $LS_2$ , up to the nominal mean displacement  $u_{me-6} = 2.5$  corresponding to the  $LS_6$ . The model's respective lateral force-mean displacement response diagram was recorded and schematized in Fig. 6(a). More excellent dispersion of the results did observe in the last three limit states. These results did attribute to the last damage states corresponding to the model collapse.

The residual displacement range ( $[u_r]$ ) corresponding to each limit state was defined proportionally to the inelastic displacement of the model ( $\mu$ ), as summarized in the fifth row of Table 6. Thus, the nominal residual displacement  $u_{r-2} = 0.30\mu$  corresponding to the  $LS_2$ , the nominal residual displacement  $u_{r-3} = 0.25\mu$  corresponding to the  $LS_3$ , up the nominal residual displacement  $u_{r-6} = 0.10\mu$  corresponding to the  $LS_6$ . The model's respective lateral force-residual displacement response diagram was recorded and schematized in Fig. 6(b). The residual displacement results exhibited did not remain constant for all limit states. In the first limit states, up to 55% of the  $\mu$  did develop, and 45% of the  $\mu$  did develop in the last three limit states. These results did likely attribute to the fact that in the first three limit states, the material model is concrete and reinforcing steel, which contributes to strength, unlike the last three limit states in which the material model did only reinforce steel; in addition to the large dispersion of results that were observed in the amplitude and mean displacement calculations indicated above.

The  $[u_{cal}]$  was defined based on the mean displacement and standard deviation,  $[u_{me} - \sigma, u_{me} + \sigma]$ , for each limit state and has been summarized in the sixth row of Table 6. Thus, the nominal model displacement  $[u_{cal-1}] = [0, 0.9]$ , corresponding to the  $LS_1$ ; the nominal model displacement  $[u_{cal-2}] = [0.3, 1.5]$ , corresponding to the  $LS_2$ ; up to the nominal model displacement  $[u_{cal-6}] = [1.9, 2.9]$  corresponding to the  $LS_6$ . The model's respective lateral force-model displacement result response diagram was recorded and schematized in Fig. 6(c). The  $[u_{cal}]$  reflected the dispersion of results and lower inelastic displacement in the last three limit states indicated above; however, it exhibited homogeneity in the amplitude of the displacement intervals, on average between 1 and 1.1. These results did attribute to the fact that it would only reflect the theoretical, analytical model.





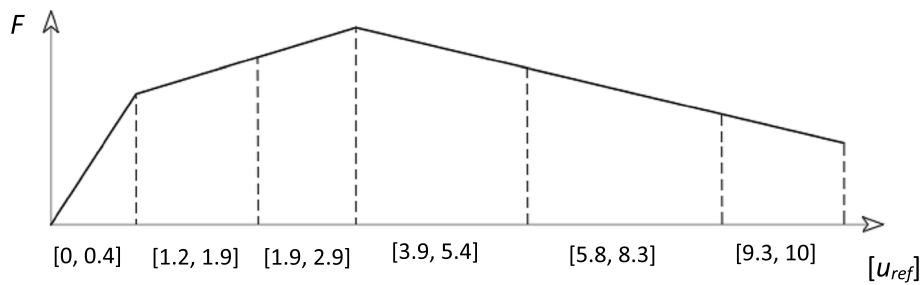
**Fig. 6** Model displacements

#### 4.2 Reference displacement ( $u_{ref}$ )

The displacements of experimental models of reference RC bridge piers indicated in Table 1 did adapt to the proposed six displacement intervals and did summarize in the seventh row of Table 6. Thus, the nominal reference displacement  $[u_{ref-1}] = [0, 0.4]$ , corresponding to the  $LS_1$ ; the nominal reference displacement  $[u_{ref-2}] = [1.2, 1.9]$ , corresponding to the  $LS_2$ ; up to the nominal reference displacement  $[u_{ref-6}] = [9.3, 10]$  corresponding to the  $LS_6$ . The model's respective lateral force-model displacement result response diagram was recorded and schematized in Fig. 7. A homogeneous amplitude of the displacement intervals was not observed as in the displacement intervals of the model, especially in the last three limit states. These results, too, were probably attributed to the last damage states corresponding to the model's collapse.

#### 4.3 RCBPM displacement ( $u$ )

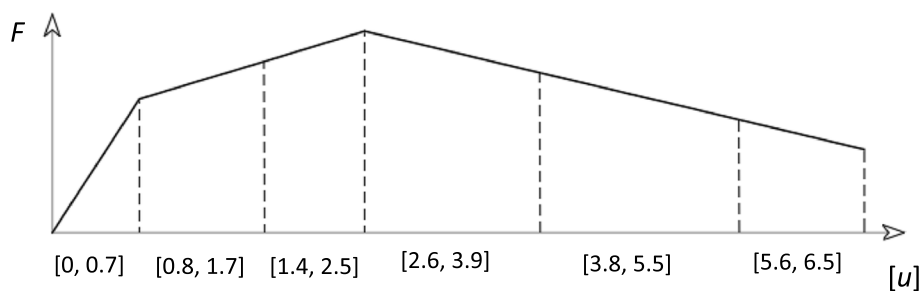
Note that the results revealed that the nominal model displacement  $[u_{cal-1}] = [0, 0.9]$  was not that different from that of the nominal reference displacement  $[u_{ref-1}] = [0,$



**Fig. 7** Reference displacements

0.4]; the nominal model displacement  $[u_{cal-2}] = [0.3, 1.5]$  was not that different from that of the nominal reference displacement  $[u_{ref-2}] = [1.2, 1.9]$ ; and the nominal model displacement  $[u_{cal-3}] = [0.9, 2]$ , was not that different from that of the nominal reference displacement  $[u_{ref-3}] = [1.9, 2.9]$ . These results did probably attribute to the fact that only in the first three limit states did the developed theoretical, analytical model have a good approximation with the reference experimental models that did already note the uniform amplitude of the displacement intervals in the lesser dispersion of the average displacements and the more remarkable development of the inelastic displacement. Therefore, the seismic performance response based on the displacement of the RCBPM was quantified, thus: the nominal displacement  $[u_1] = [0, 0.7]$  mean of  $[0, 0.9]$  and  $[0, 0.4]$ , corresponding to the  $LS_1$ ; the nominal displacement  $[u_2] = [0.8, 1.7]$  mean of  $[0.3, 1.5]$  and  $[1.2, 1.9]$ , corresponding to  $LS_2$ ; and up to nominal displacement  $[u_3] = [1.4, 2.5]$  mean of  $[0.9, 2]$  and  $[1.9, 2.9]$ , corresponding to  $LS_3$ ; as specified in the last row of Table 6 and as illustrated in Fig. 8.

While the nominal reference displacement  $[u_{ref-4}] = [3.9, 5.4]$  was higher than that of the nominal model displacement  $[u_{cal-4}] = [1.3, 2.4]$ ; also the nominal reference displacement  $[u_{ref-5}] = [5.8, 8.3]$ , was higher than that of the nominal model displacement  $[u_{cal-5}] = [1.7, 2.7]$ . The nominal reference displacement  $[u_{ref-6}] = [9.3, 10]$  was higher than that of the nominal model displacement  $[u_{cal-6}] = [1.9, 2.9]$ . These results did probably attribute to the fact that the developed theoretical, analytical model could have better approximated the last three limit states with the reference experimental models; what did already note in the greater amplitude of the displacement intervals, the more excellent dispersion of the mean displacements, and the lesser development of the inelastic displacement. However, the seismic performance response based on the displacement of the RCBPM was also quantified, thus: the nominal displacement  $[u_4] = [2.6, 3.9]$  mean of  $[1.3, 2.4]$  and  $[3.9, 5.4]$ , corresponding to the  $LS_4$ ; the nominal displacement  $[u_5] = [3.8,$



**Fig. 8** RCBPM displacements

5.5] mean of [1.7, 2.7] and [5.8, 8.3], corresponding to the  $LS_5$ ; and up to the nominal displacement  $[u_6] = [5.6, 6.5]$  mean of [1.9, 2.9] and [9.3, 10], corresponding to the  $LS_6$ ; as specified in the last row of Table 6 and as illustrated in Fig. 8.

#### 4.4 Displacement prediction

A multiple linear regression analysis derived a formula to relate the displacement with the eleven input parameters. The derived multiple linear regression formula is as Eq. (5), shown as the displacement prediction equation for RCBPM corresponding to the  $[u_3]$ .

With Eq. (5), 13,830 displacement results did obtain and compared with the 4608 displacement results of the developed model, finding discrepancies of around 20%, as illustrated in Fig. 9.

$$u_3 = - (8 * 10^{-6}) \frac{L}{D} - 0.00002d_l - 0.0003\Phi + 0.0001f_c + 0.0004s + (3.2 * 10^{-6})f_y + 0.0022\rho_l - 0.0376r - 0.00004P - 0.0001dt - (6.1 * 10^{-14})k_s + 0.0170 \tag{5}$$

As an example of the application of the respective prediction equation, the displacement of the RC bridge pier was calculated (Fig. 6 (a), experimental specimen A, studied by Hung et al. (2011). An experimental study on the rocking response of bridge piers with spread footing foundations. *Earthquake Engineering and Structural Dynamics*. <https://doi.org/10.1002/eqe.1057>). The specified displacement of the specimen ( $u_{3-specimen}$ ) was 1.8%; however, the measurement results revealed that the displacement calculated with the respective prediction equation Eq. (6) was  $u_3 = 2.1\%$ . Therefore, the displacement of the experimental model of the RC bridge pier,  $u_{3-specimen} = 1.8\%$ , was close to that calculated with the respective prediction equation as  $u_3 = 2.1\%$ ; in addition, it did found that the displacements  $u_{3-specimen}$  and  $u_3$ , within the displacement interval proposed as  $[u_3] = [1.4\%, 2.5\%]$ .

As another example of the application of the respective prediction equation, the displacement of the RC bridge pier was calculated (Fig. 7 (a), studied by Barbosa (2015). Seismic performance of high-strength steel RC bridge columns. *American Society of Civil Engineers*. [https://doi.org/10.1061/\(ASCE\)BE.1943-5592.0000769](https://doi.org/10.1061/(ASCE)BE.1943-5592.0000769)). The specified displacement of the specimen ( $u_{3-specimen}$ ) was 2.1%; however, the measurement results

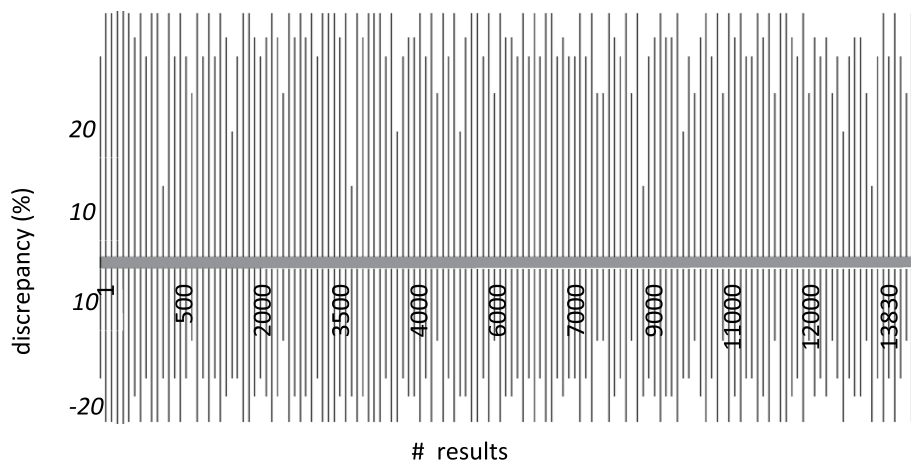
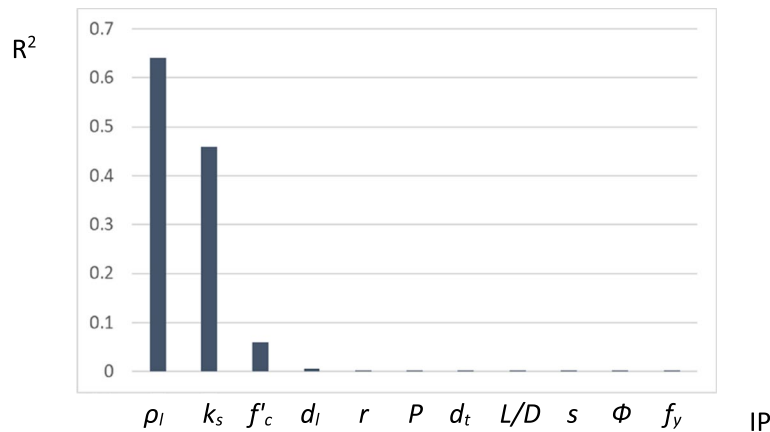


Fig. 9 Discrepancy in lateral displacement results



**Fig. 10** Relative importance factors for input parameters

**Table 7** Input parameters relevant and irrelevant

Input parameters				
R <sup>2</sup> :	ρ <sub>l</sub> 0.6366	k <sub>s</sub> 0.464		f <sub>c</sub> , P, L/D, Φ, r, d <sub>t</sub> , s, f <sub>y</sub> , d <sub>l</sub> Σ = 0.07
Rr <sup>2</sup> :	Φ 0.5058	s 0.5095	d <sub>l</sub> 0.5128	f <sub>c</sub> , P, L/D, r, d <sub>t</sub> , f <sub>y</sub> , k <sub>s</sub> , ρ <sub>l</sub> 0.5128
	@ 0.5059	@ 0.5096	@ 0.5129	@ 0.3239

revealed that the displacement calculated with the respective prediction equation Eq. (7) was  $u_3 = 2\%$ . Therefore, the displacement of the experimental model of the RC bridge pier,  $u_{3-specimen} = 2.1\%$ , was close to that calculated with the respective prediction equation as  $u_3 = 2\%$ ; in addition, it did find that the displacements  $u_{3-specimen}$  and  $u_3$ , within the displacement interval proposed as  $[u_3] = [1.4\%, 2.5\%]$ .

$$\begin{aligned}
 u_{3-specimen} = & - (8 \times 10^{-6}) * 6 - 0.00002 * 6 - 0.0003 * 1 + 0.0001 * 29 + 0.0004 * 0.1 \\
 & + (3.2 \times 10^{-6}) * 420 + 0.0022 * 2.63 - 0.0376 * 0.0254 - 0.00004 * 15 - 0.0001 * 3 \quad (6) \\
 & - (6.1 \times 10^{-14}) * (5 \times 10^{10}) + 0.0170 = 0.021 \approx 0.018
 \end{aligned}$$

$$\begin{aligned}
 u_{3-specimen} = & - (8 \times 10^{-6}) * 6 - 0.00002 * 6 - 0.0003 * 1.1 + 0.0001 * 32.1 + 0.0004 * 0.05 \\
 & + (3.2 \times 10^{-6}) * 420 + 0.0022 * 2.19 - 0.0376 * 0.0318 - 0.00004 * 5 - 0.0001 * 3 \quad (7) \\
 & - (6.1 \times 10^{-14}) * (5 \times 10^{10}) + 0.0170 = 0.020 \approx 0.021
 \end{aligned}$$

#### 4.5 Parametric study

##### 4.5.1 Influence of IP of response of seismic performance of RCBPM

The values of  $R^2$  obtained from the respective simple linear regression analysis of the 13,830 results corresponding to the LS<sub>3</sub>, such as  $R^2 = 0.6366$  for the  $\rho_l$  input parameter,  $R^2 = 0.464$  for the  $k_s$  input parameter,  $R^2 = 0.0553$  for the  $f_c$  input

parameter,  $R^2 = 0.0053$  for the  $d_l$  input parameter,  $R^2 = 0.0021$  for the  $r$  input parameter; up to  $R^2 = 7 \cdot 10^{-5}$  for the  $f_y$  input parameter. Therefore, the  $\rho_l$  input parameter and the  $k_s$  input parameter were the ones with the most significant influence on the response of the seismic performance of the RCBPM. The other nine ( $f'_c$ ,  $P$ ,  $L/D$ ,  $\Phi$ ,  $r$ ,  $d_p$ ,  $s$ ,  $f_y$ ,  $d_l$ ) input parameters reached shallow values of  $R^2$  (less than 0.07), which have no statistical significance, practically meaningless, as specified in Fig. 10 and third row of Table 7.

The values of  $Rr^2$  did obtain from the respective multiple linear regression analysis of the 4608 results corresponding to the  $LS_3$ . The  $Rr^2 = 0.5128$  considering all eleven input parameters ( $\rho_l$ ,  $k_s$ ,  $f'_c$ ,  $P$ ,  $L/D$ ,  $\Phi$ ,  $r$ ,  $d_p$ ,  $s$ ,  $f_y$ ,  $d_l$ ); the  $Rr^2 = 0.5129$  considering ten input parameters ( $\rho_l$ ,  $k_s$ ,  $f'_c$ ,  $P$ ,  $L/D$ ,  $\Phi$ ,  $r$ ,  $d_p$ ,  $s$ ,  $f_y$ ); the  $Rr^2 = 0.5095$  considering nine input parameters ( $\rho_l$ ,  $k_s$ ,  $f'_c$ ,  $P$ ,  $L/D$ ,  $\Phi$ ,  $r$ ,  $d_p$ ,  $s$ ); up to  $Rr^2 = 0.3239$  a single input parameter ( $\rho_l$ ). The values of  $Rr^2$  obtained are less than 1, which indicates that it is not so easy to predict the displacement of the RCBPM.

By ignoring the input parameter  $\Phi$  in the multiple linear regression analysis performed, the value  $Rr^2 = 0.5058$  increased to  $Rr^2 = 0.5059$ ; by ignoring the input parameter  $s$  in the multiple linear regression analysis performed, the value  $Rr^2 = 0.5095$  increased to  $Rr^2 = 0.5096$ ; by ignoring the input parameter  $d_l$  in the multiple linear regression analysis performed, the value  $Rr^2 = 0.5128$  increased to  $Rr^2 = 0.5129$ . Therefore, the irrelevance of the four parameters ( $\Phi$ ,  $s$ , and  $d_l$ ) cannot be determined since these increases reached shallow values of  $Rr^2$  (less than 0.01), which have no statistical significance, practically meaningless, as the specified fifth row of Table 7.

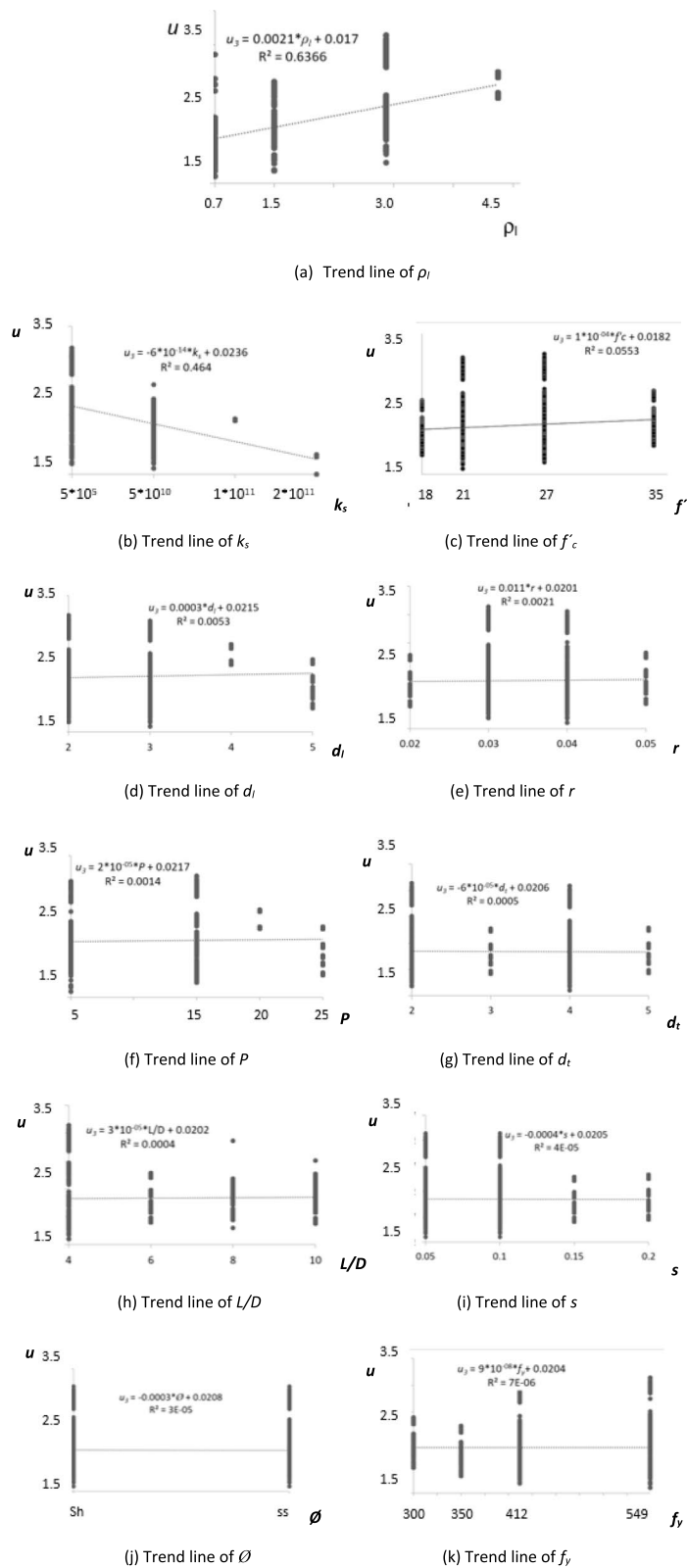
#### 4.5.2 IP trend analysis

A clear increasing trend did found; as the longitudinal reinforcement ratio increased, the displacement tended to increase, as illustrated in Fig. 11(a). It is likely because excessive longitudinal steel bars did not use (0.7%, 1.5%, 3%, and 4.5%), and the failure mode did not change from ductile to fragile, which did not deteriorate displacement capacity.

The coefficient of subgrade reaction refers to the settlement ratio of the ground caused by the load acting on the foundation. It represents how much the ground can withstand when subjected to loads from the structure, assuming the ground behaves like a spring. The coefficient of subgrade reaction is a constant that represents the stiffness of the ground. A larger coefficient of subgrade reaction indicates that the soil is more stable, dense, less compressible, and has a higher bearing capacity.

Also, a clear decreasing trend did found; as the reaction coefficient of the subgrade increased, the displacement tended to decrease, as illustrated in Fig. 11(b). It was likely because a low value of the reaction coefficient of the subgrade represented a flexible soil that makes the foundation of an RC bridge pier unstable.

Thus, the Fig. 11(c) up (k) could not define the trend line for the other nine input parameters ( $f'_c$ ,  $d_p$ ,  $r$ ,  $P$ ,  $d_p$ ,  $L/D$ ,  $s$ ,  $\Phi$ ,  $f_y$ ), since the data is sparse, as reflected in the shallow values of  $R^2$  (less than 0.07), which have no statistical significance, practically meaningless.



**Fig. 11** Linear regression analysis

## 5 Conclusions

This article presents the response of the seismic performance of the reinforced concrete bridge pier model was evaluated in terms of displacement, taking into account eleven input parameters for six limit states, obtaining the following conclusions:

- (i) The range of the displacement in terms of drift was found: for the cracking displacement  $[u_1] = [0, 0.7\%]$ , corresponding to the cracking limit state; for the yielding displacement  $[u_2] = [0.8\%, 1.7\%]$ , corresponding to the yielding limit state; for the spalling displacement  $[u_3] = [1.4\%, 2.5\%]$ , corresponding to the spalling limit state; for the crushing displacement  $[u_4] = [2.6\%, 3.9\%]$ , corresponding to the crushing limit state; for the buckling displacement  $[u_5] = [3.8\%, 5.5\%]$ , corresponding to the buckling limit state; and for the fracturing displacement  $[u_6] = [5.6\%, 6.5\%]$ , corresponding to the fracturing limit state. It can do use to evaluate expected displacements in reinforced concrete bridge piers.
- (ii) The derived prediction equation for spalling displacement showed an excellent approximation, around 20%, compared to the model displacement. It can do use for the initial calculation of referential spalling displacements.
- (iii) The pier aspect ratio and coefficient of subgrade reaction; were the two most influential in the response of the seismic performance of the reinforced concrete bridge piers, with coefficient of determination values of 64% and 46%, respectively; however, it did not approach 100%, indicating that displacement is not as easy to predict.
- (iv) The concrete compressive strength, the yield stress of reinforcing steel, the concrete cover thickness, the configuration of the transverse reinforcement, the spacing of the transverse reinforcing steel, the transversal diameter of the transverse reinforcing steel, the longitudinal reinforcement ratio, the transversal diameter of the longitudinal reinforcing steel, and the axial load ratio; were the nine input parameters less influential in the response of the seismic performance of the reinforced concrete bridge piers, with the coefficient of determination values up to a total of 7%, indicating their low influence on displacement and were statistically insignificant.

### Acknowledgements

The authors would like to acknowledge the National University of San Cristobal de Huamanga (Peru) for the financial support provided for carrying on his doctoral studies. Also, we would like to thank the Engineering Doctoral Program at the Pontifical Catholic University of Peru for the support received.

### Authors' contributions

Javier Taïpe conceived this study, participated in its design and coordination, and reviewed and revised the manuscript. Victor Fernandez-Davila participated in the analysis of the test data, and revised of the manuscript. All the authors read and approved the final manuscript.

### Funding

None.

### Availability of data and materials

The data and materials generated or used during the study are available from the corresponding author by request.

### Declarations

#### Competing interests

The author(s) declared no potential conflicts of interest with respect to the research, authorship, and/or publication of this article.

Received: 1 June 2023 Accepted: 30 July 2023

Published online: 30 August 2023

**References**

- Aamir Baig M, Imteyaz Ansari M, Islam N, Umair M (2022) Damage assessment of circular bridge pier incorporating high-strength steel reinforcement under near-fault ground motions. *Mater Today: Proc* 64:488–498. <https://doi.org/10.1016/j.matpr.2022.04.964>
- Abdallah AE, El-Salakawy EF (2022) Seismic performance of GFRP-RC circular columns with different aspect ratios and concrete strengths. *Eng Struct* 257:114092. <https://doi.org/10.1016/j.engstruct.2022.114092>
- AfsarDizaj E, Kashani MM (2020) Numerical investigation of the influence of cross-sectional shape and corrosion damage on failure mechanisms of RC bridge piers under earthquake loading. *Bull Earthq Eng*. <https://doi.org/10.1007/s10518-020-00883-3>
- Ali AH, Mohamed HM, Chaallal O, Benmokrane B, Ghrib F (2018) Shear resistance of RC circular members with FRP discrete hoops versus spirals. *Eng Struct* 174(August):688–700. <https://doi.org/10.1016/j.engstruct.2018.07.060>
- Anand V, Satish Kumar KS (2018) Seismic soil-structure interaction: a state-of-the-art review. *Structures*. <https://doi.org/10.1016/j.jistruc.2018.10.009>
- Barbosa AR (2015) Seismic performance of high-strength steel rc bridge columns. *Am Soc Civil Eng*. [https://doi.org/10.1061/\(ASCE\)BE.1943-5592.0000769](https://doi.org/10.1061/(ASCE)BE.1943-5592.0000769)
- Bouazza H, Djelil M, Matallah M (2022) On the relevance of incorporating bar slip, bar buckling and low-cycle fatigue effects in seismic fragility assessment of RC bridge piers. *Eng Struct* 256:114032. <https://doi.org/10.1016/j.engstruct.2022.114032>
- Carrasquilla-Batista A, Chacón-Rodríguez A, Núñez-Montero K, Gómez-Espinoza O, Valverde-Cerdas J, Guerrero-Barrantes M (2016) Simple and multiple linear regression: application in the prediction of natural variables related to microalgal growth. *Technol Magazine* 29(8):33. <https://doi.org/10.18845/tm.v29i8.2983>
- Cassese P, De Risi MT, Verderame GM (2019) A modelling approach for existing shear-critical RC bridge piers with hollow rectangular cross section under lateral loads. *Bull Earthq Eng*. <https://doi.org/10.1007/s10518-018-0429-2>
- d'Avila MPS, Lenti L, Gobbi S, Fares R (2022) Reduced T-shaped soil domain for nonlinear dynamic soil-bridge interaction analysis. *Adv Bridge Eng* 3(1):1–15. <https://doi.org/10.1186/s43251-022-00057-y>
- Ding Y, Wu D, Su J, Li ZX, Zong L, Feng K (2021) Experimental and numerical investigations on seismic performance of RC bridge piers considering buckling and low-cycle fatigue of high-strength steel bars. *Eng Struct* 227:111464. <https://doi.org/10.1016/j.engstruct.2020.111464>
- Fu JY, Ge X, Li JT, Sun ZG, Wang DS (2022) Seismic performance of concrete bridge piers reinforced by stainless steel bars: A quasi-static experimental study. *Eng Struct* 266:114507. <https://doi.org/10.1016/j.engstruct.2022.114507>
- Hung H, Liu K, Ho T, Chang K (2011) An experimental study on the rocking response of bridge piers with spread footing foundations. *Earthquake Eng Struct Dynam*. <https://doi.org/10.1002/eqe.1057>
- Jiao C, Zhu G, Long P, Shi X (2019) Seismic performance of RC circular piers with medium and low shear span ratio under compression, bending and torsion action. In: 3rd International Conference on Smart City and Systems Engineering, ICSCSE 2018. pp. 368–374. <https://doi.org/10.1109/ICSCSE.2018.00081>
- Kashani MM, Ge X, Dietz MS, Crewe AJ, Alexander NA (2019) Significance of non-stationary characteristics of ground-motion on structural damage: shaking table study. *Bull Earthq Eng*. <https://doi.org/10.1007/s10518-019-00668-3>
- Kehila F, Remki M (2015) Fragility curves and axial force effect on improved damage index of reinforced concrete bridges piers. Conference: international conference on civil and environmental engineering (Cappadocia-2015), Nevşehir
- Li RW, Zhou DY, Wu H (2020) Experimental and numerical study on impact resistance of RC bridge piers under lateral impact loading. *Eng Failure Anal* 109:1–19. <https://doi.org/10.1016/j.engfailanal.2019.104319>
- Li Y, Zong Z, Yang B, Lin Y, Lin J (2020) Research on longitudinal collapse mode and control of the continuous bridge under strong seismic excitations. *Appl Sci (Switzerland)* 10(17):6049. <https://doi.org/10.3390/app10176049>
- Liu L, Yang X, Yan B, Miao S (2022) Dynamic Responses of RC Girder Bridge under Heavy Truck and Seismic Loads Combined. *Sustainability (Switzerland)* 14(15):9263. <https://doi.org/10.3390/su14159263>
- Ou Y-C, Wu J-W, Pratiwi AY (2022) Effect of the concrete cover thickness ratio on the post-yield stiffness of bridge columns with partially unbonded unstressed steel strands. *Adv Bridge Eng* 3(1):13. <https://doi.org/10.1186/s43251-022-00060-3>
- Pang Y, Li L (2018) Seismic collapse assessment of bridge piers constructed with steel fibers reinforced concrete. *PLoS ONE* 13(7):1–20. <https://doi.org/10.1371/journal.pone.0200072>
- Park S, Koem C, Shim C (2020) Quantitative definition of seismic performance levels for precast bridge piers with continuous reinforcement. *Adv Civil Eng* 2020:1–21. <https://doi.org/10.1155/2020/4087532>
- Ren J, Xu Q, Chen G, Yu X, Gong S, Lu Y (2022) Full-scale experimental study of the seismic performance of pretensioned spun high-strength concrete piles. *Soil Dyn Earthq Eng* 162:107467. <https://doi.org/10.1016/j.soildyn.2022.107467>
- Shelman A, Sritharan S (2014) A critical review of column confinement reinforcement used in current seismic bridge design practice. Iowa state university. Department of civil, construction and environmental engineering. California department of transportation, division of engineering services. <https://books.google.com.pe/books?id=8MFOkQEJ7K4C>
- Shi X, Song LL, Guo T, Pan ZH (2022) Seismic design of self-centering bridge piers considering soil-structure interaction. *Structures* 43:1819–1833. <https://doi.org/10.1016/j.jistruc.2022.07.055>
- Srivastava C, Pandikkadavath MS, Mangalathu S (2022) Effect of material variability on the seismic response of reinforced concrete box-girder bridges for different pier heights. *Mater Today: Proc* 65:564–571. <https://doi.org/10.1016/j.matpr.2022.03.186>



- Su J, Wang J, Bai Z et al (2015) Influence of reinforcement buckling on the seismic performance of reinforced concrete columns. *Eng Struct*. <https://doi.org/10.1016/j.engstruct.2015.09.007>
- Su J, Wang J, Li Z (2019) Effect of reinforcement grade and concrete strength on seismic performance of reinforced concrete bridge piers. *Eng Struct*. <https://doi.org/10.1016/j.engstruct.2019.109512>
- Su J, Li Z, Wang J et al (2020) Numerical simulation and damage analysis of RC bridge piers reinforced with varying yield strength steel reinforcement. *Soil Dyn Earthq Eng*. <https://doi.org/10.1016/j.soildyn.2019.106007>
- Su J, Li ZX, Prasad DR, Li C, Wang F (2021) Comparative study on seismic vulnerability of RC bridge piers reinforced with normal and high-strength steel bars. *Structures*. <https://doi.org/10.1016/j.istruc.2020.12.048>
- Su J, Dhakal R P, Wang J, et al. (2017a) Seismic performance of RC bridge piers reinforced with varying yield strength steel. *Earthq Struct*. <https://doi.org/10.12989/eas.2017.12.2.201>
- Su J, Dhakal R P, Wang J. (2017b) Fiber-based damage analysis of reinforced concrete bridge piers[J]. *Soil Dyn Earthq Eng*. <https://doi.org/10.1016/j.soildyn.2017b.01.029>
- Tan JS, Elbaz K, Wang ZF, Shen JS, Chen J (2020) Lessons learnt from bridge collapse: A view of sustainable management. *Sustainability (switzerland)* 12(3):1–16. <https://doi.org/10.3390/su12031205>
- Todorov B, Billah AHMM (2021) Seismic fragility and damage assessment of reinforced concrete bridge pier under long-duration, near-fault, and far-field ground motions. *Structures* 31:671–685. <https://doi.org/10.1016/j.istruc.2021.02.019>
- Todorov B, Muntasir Billah AHM (2022a) Machine learning driven seismic performance limit state identification for performance-based seismic design of bridge piers. *Eng Struct* 255:113919. <https://doi.org/10.1016/j.engstruct.2022.113919>
- Todorov B, Muntasir Billah AHM (2022b) Post-earthquake seismic capacity estimation of reinforced concrete bridge piers using Machine learning techniques. *Structures* 41:1190–1206. <https://doi.org/10.1016/j.istruc.2022.05.067>
- Tran NL, Nguyen TH, Phan VT, Nguyen DD (2020) Seismic fragility analysis of reinforced concrete piers of steel box girder bridges: A parametric study. *Mater Today: Proc* 38:2310–2315. <https://doi.org/10.1016/j.matpr.2020.06.414>
- Wang F, Hua J, Xue X, Ding Z, Lyu Y, Liu Q (2022) Low-cycle fatigue performance of bimetallic steel bar considering the effect of inelastic buckling. *Construct Build Mater* 351:128787. <https://doi.org/10.1016/j.conbuildmat.2022.128787>
- Wu D, Ding Y, Su J, Li ZX, Zong L (2022) Investigation on low-cycle fatigue performance of high-strength steel bars including the effect of inelastic buckling. *Eng Struct* 272:114974. <https://doi.org/10.1016/j.engstruct.2022.114974>
- Xiamuxi A, Maimaitimin M, Liu X (2019) Experimental study on transverse reinforcements of reinforced concrete-filled steel tubular column. *Eng Struct*. <https://doi.org/10.1016/j.engstruct.2019.109422>
- Zhong J, Ni M, Hu H, Yuan W, Yuan H, Pang Y (2022) Uncoupled multivariate power models for estimating performance-based seismic damage states of column curvature ductility. *Structures* 36:752–764. <https://doi.org/10.1016/j.istruc.2021.12.041>
- Zhou J, Kunnath SK (2022) Capacity limit states for nonductile bridge columns. *Pacific Earthquake Engineering Research Center College of Engineering University of California, Berkeley*. <https://peer.berkeley.edu/publications/2022-01>
- Zignago D, Barbato M (2019) Parametric study on the effect of steel confinement in short bridge piers retrofitted with externally-wrapped FRP. *MATEC Web of Conferences*, <https://doi.org/10.1051/mateconf/201927101012>

## Publisher's Note

Springer Nature remains neutral with regard to jurisdictional claims in published maps and institutional affiliations.

Submit your manuscript to a SpringerOpen<sup>®</sup> journal and benefit from:

- Convenient online submission
- Rigorous peer review
- Open access: articles freely available online
- High visibility within the field
- Retaining the copyright to your article

---

Submit your next manuscript at ► [springeropen.com](https://www.springeropen.com)

---